

## Identification of Carbon Stars from LAMOST DR7

LINLIN LI <sup>1</sup>, KECHENG ZHANG,<sup>1</sup> WENYUAN CUI <sup>1</sup>, JIANRONG SHI <sup>2</sup>, WEI JI <sup>3,4</sup>, ZHENYAN HUO,<sup>1</sup> YAWEI GAO,<sup>1</sup>  
SHUAI ZHANG <sup>1</sup> AND MINGXU SUN <sup>1</sup>

<sup>1</sup>*Department of Physics, Hebei Normal University, Shijiazhuang 050024, China; wenyuancui@126.com*

<sup>2</sup>*Key Lab of Optical Astronomy, National Astronomical Observatories, Chinese Academy of Sciences  
A20 Datun Road, Chaoyang, Beijing 100101, China*

<sup>3</sup>*Key Laboratory of Space Astronomy and Technology, National Astronomical Observatories, CAS,  
Beijing 100101, China*

<sup>4</sup>*School of Astronomy and Space Science, University of Chinese Academy of Sciences, Beijing 100049, Peoples Republic of China*

### ABSTRACT

Carbon stars are excellent kinematic tracers of galaxies and play important roles in understanding the evolution of the Galaxy. Therefore, it is worthwhile to search for them in a large amount of spectra. In this work, we build a new carbon star catalog based on the LAMOST DR7 spectra. The catalog contains 4542 spectra of 3546 carbon stars, identified through line index and near-infrared color-color diagrams. Through visual inspection of the spectra, we further subclassify them into 925 C–H, 384 C–R, 608 C–N, and 1292 Ba stars. However, 437 stars could not be sub-classified due to their low signal-to-noise. Moreover, by comparing with LAMOST DR7 pipeline we find 567 more carbon stars and visually sub-classify them. We find that on the  $J-H$  vs.  $H-K_s$  two-color diagram, C–N stars can be reliably distinguished from the other three sub-types. Additionally, by utilizing the Gaia distance, we study the distribution of carbon stars in the H-R diagram and identify 258 dwarf carbon stars by the criterion  $M_G > 5.0$  mag. Finally, we present the spatial distribution in Galactic coordinates of the 3546 carbon stars. The majority of C–N, C–R, and Ba stars are distributed at low Galactic latitudes, while most C–H and dC stars distribute at high Galactic latitudes.

*Keywords:* catalogs(205); carbon stars(199); Astrostatistics(1882); Sky surveys(1464)

### 1. INTRODUCTION

Carbon stars are rare and peculiar objects first discovered by Secchi (1869), and characterized by strong carbon molecular bands, such as CH, CN, and C<sub>2</sub>, in their optical spectra. They usually have similar temperature and luminosity with late G, K and M stars, while showing higher carbon abundance than oxygen (i.e., C/O > 1) (Keenan 1993). The atmospheric carbon of dwarf carbon stars is thought to be obtained by mass transfer from an asymptotic giant branch (AGB) companion, which is now a white dwarf star (Iben & Renzini 1983; Boothroyd & Sackmann 1988). Cool and luminous carbon stars acquire their carbon enrichment through the ongoing third dredge-up during the AGB phase.

According to their different spectral features, carbon stars can be classified into different sub-classes (Keenan 1993; Barnbaum et al. 1996), including C–H, C–R, C–N, C–J and Ba stars. The classification criteria have been discussed by Li et al. (2018). They can also be divided into giant and dwarf carbon stars (dC) depending on their brightness. Note that these classifications have no direct relationship with their origin. It is well known that most stars belong to binary systems (Duchêne & Kraus 2013) and they are no exception for carbon stars. Almost all Ba and C–H stars are binaries (McClure et al. 1980; McClure 1983; Jorissen et al. 2016; Escorza & De Rosa 2023; Goswami & Goswami 2023). Aikman & McClure (1984) carried out a series of radial velocity monitoring for C–N stars, and found signs of binary companions for C–N stars. However, McClure (1997) did not find any evidence of binary for 22 C–R stars after 16 years of radial velocity monitoring.

Carbon dwarfs have been proven to be the most common type (Green 2000), but the discovery of carbon dwarfs occurred much later than that of carbon giants. Most of the known carbon stars so far are giants due to the lower luminosity of dC stars. Dahn et al. (1977) discovered a carbon star (G77-61), which, based on its parallax and spatial

motion, is a low-luminosity object located on the M-dwarf sequence in the H-R diagram, and G77-61 now appears to be a prototype of carbon dwarfs. More dC stars are needed to explain their origins and the relationship with the carbon giants.

Among the sub-types of carbon stars, the C–N and C–H stars receive more attention. Since C–N stars are mostly in the AGB stage, they are intrinsically bright and can be easily identified by the strong carbon molecular bands in their spectra. They have been used as kinematic probes of the Galaxy at large distances (Demers & Battinelli 2007; Battinelli et al. 2013). Additionally, the small dispersion in the absolute magnitude of C–N stars allows them to be used as reliable candles to measure the distance of extragalaxies (Ripoche et al. 2020; Parada et al. 2023). C–H stars are metal-poor and can be found mostly in halo populations (Goswami 2005). A larger sample of C–H stars is very helpful in improving our knowledge about the formation history of the stellar halo. Moreover, their more metal-poor counterparts, carbon-enhanced metal-poor (CEMP) stars (Abate et al. 2016; Shejeelammal & Goswami 2022), provide essential information about the early Galactic chemical evolution and the nature of the very first stars.

So far, many works have been carried out for systematically identifying carbon stars, e.g., Alksnis et al. (2001) published a catalog of 6891 carbon stars, which is an updated and revised version of Stephenson’s catalog of Galactic cool carbon stars (Stephenson 1973, 1989), Totten & Irwin (1998) reported 48 cool (N-type) carbon stars, and Christlieb et al. (2001) presented a sample of 403 faint high-latitude carbon (FHLC) stars selected from the digitized objective plasma plates of the Hamburg/ESO Survey (HES). Over the next ten years, several studies systematically searched for carbon stars from the Sloan Digital Sky Survey (SDSS) (Margon et al. 2002; Downes et al. 2004; Green 2013; Si et al. 2014). Restricted to the sky survey area of SDSS, the identified carbon stars are mainly FHLC stars. Since the data release of the Large Sky Area Multi-Object Fiber Spectroscopy Telescope (LAMOST) in the year 2011, new carbon stars were reported from its massive number of spectra, e.g., Si et al. (2015) used machine learning to identify 183 carbon stars from the LAMOST pilot survey data, Ji et al. (2016) obtained a sample of 894 carbon stars from LAMOST DR2 using multiple line index spaces and  $JHK_s$  color-magnitude diagram, and Li et al. (2018) reported 2651 carbon stars from LAMOST DR4 using machine learning.

In this paper, our goal is to use the LAMOST DR7 dataset to expand the sample of carbon stars. This paper is organized as follows. In Section 2, we introduce the dataset of LAMOST DR7. In Section 3, we describe the identification method and the process for searching for carbon stars, and we provide the final results. In section 4, we discuss the distribution of carbon stars in the  $J-H$  vs.  $H-K_s$  and  $H-R$  diagrams, in which we identify 258 possible dC stars, and the spatial distribution of the carbon stars is also shown in this section. Finally, a brief summary is given in Section 5.

## 2. DATA

### 2.1. LAMOST DR7

LAMOST, also called the Guo Shou Jing telescope, is a 4 m reflective Schmidt telescope with 4000 fibers in a 20 square degree focal plane (Cui et al. 2012; Zhao et al. 2012). LAMOST can simultaneously obtain the spectra of 4000 targets in a single exposure, and its resolution is  $\sim 1800$  for the low resolution mode.

In June 2019, LAMOST completed its seventh year of sky survey. On March 31, 2020, the LAMOST DR7 dataset, including the pilot survey and the seven years regular survey, was officially released to astronomers. In this release, it comprises 4922 low resolution observation plates. The DR7 dataset contains 14,487,406 spectra, including 10,599,979 low resolution spectra, and 1,008,710 nontime domain and 2,878,717 time domain medium resolution spectra. In the LAMOST DR7 Low-Resolution Spectroscopic (LRS) General Catalog<sup>1</sup>, there are 4402 spectra of 3565 stars labeled as carbon for the “subclass” parameter (stellar spectral type). However, the contamination rate is not presented, and no classification of the carbon stars is given. In this work, we systematically search for different types of carbon stars from more than 10 million low resolution spectra.

### 2.2. Line indices

We use the multiple line index spaces to select carbon stars, as the spectra of carbon stars are characterized by strong absorption bands of carbon-containing molecules, such as CH, C<sub>2</sub> and CN.

<sup>1</sup> <http://dr7.lamost.org/catalogue>

**Table 1.** Line Indices Definition in This Work

Name	Index Bandpass (Å)	Pseudo-continua (Å)	
(1)	(2)	(3)	
C <sub>2</sub> (4737Å)	4620–4742	4580–4620	4742–4812
C <sub>2</sub> (5165Å)	4980–5170	4930–4980	5170–5235
C <sub>2</sub> (5635Å)	5350–5640	5300–5350	5640–5700
CN(7065Å)	7065–7190	7025–7065	7190–7230
CN(7820Å)	7820–8000	7790–7820	8000–8040

The line index is defined by the following equation according to the equivalent width (Worthey et al. 1994; Liu et al. 2015):

$$EW = \int [1 - \frac{f_{line}(\lambda)}{f_{cont}(\lambda)}] d\lambda, \quad (1)$$

where,  $f_{cont}(\lambda)$  and  $f_{line}(\lambda)$  are the fluxes of the continuum and the spectral line, respectively, both of them are functions of wavelength. The line index under this definition is in Å. We measure five line indices including C<sub>2</sub>(λ 4737 Å, λ 5165 Å, and λ 5635 Å) and CN (λ 7065 Å, and λ 7820 Å). The definition of line indices is listed in Table 1.

### 3. IDENTIFICATION AND SPECTRAL CLASSIFICATION OF CARBON STARS

#### 3.1. The identification steps of carbon stars

The LAMOST DR7 dataset contains 10,599,979 low resolution spectra. In order to derive the carbon star candidates, we use multiple line index spaces to remove as many contaminants as possible.

The high signal-to-noise spectra are helpful to us to identify and classify carbon stars more accurately. Therefore, we only selected the spectra of S/N (i)>10 from LAMOST DR7, and obtained 9,060,920 stellar spectra, in which some objects have been observed in more than one epoch. In order to determine the intrinsic location of carbon stars in line index spaces, we cross-matched the known carbon star catalogs of Li et al. (2018), Ji et al. (2016), and Alksnis et al. (2001) with the selected LAMOST DR7 dataset, and found 2275, 889, and 373 carbon stars, respectively. In Figure 1, we draw all the known carbon stars and candidates in the  $EW_{CN(\lambda 7820 \text{ \AA})}$  vs.  $EW_{CN(\lambda 7065 \text{ \AA})}$  plane, and it can be seen that the distribution of known carbon stars spreads from the center to the upper right in a narrow area. In the central region around the origin point in Figure 1, different types of stars are mixed, and it is very difficult to identify the carbon stars in the highly contaminated region. Hence, we exclude the central region in the following discussion. We adopt the following empirical criteria in the  $EW_{CN(\lambda 7820 \text{ \AA})}$  vs.  $EW_{CN(\lambda 7065 \text{ \AA})}$  plane so that most of the known carbon stars are included. After this step, we get 722,171 candidates, accounting for about 8% of the total number before cutting. The criteria are:

$$\begin{aligned}
& 1.2 \times EW_{CN(\lambda 7065 \text{ \AA})} - 1.29 < EW_{CN(\lambda 7820 \text{ \AA})} \\
& < 3.8 \times EW_{CN(\lambda 7065 \text{ \AA})} + 3.0, \\
& EW_{CN(\lambda 7065 \text{ \AA})} > 0.7, \\
& EW_{CN(\lambda 7820 \text{ \AA})} > 1.0.
\end{aligned} \quad (2)$$

We further remove pollution based on the infrared color-color diagram, since previous works have shown that the distribution of carbon stars in the  $J-H$  vs.  $H-K_s$  two-color diagram is highly concentrated (Totten et al. 2000; Gigoyan et al. 2012; Si et al. 2015). The values of  $J$ ,  $H$ , and  $K_s$  for both known carbon stars and candidates are obtained by cross-identifying with the 2MASS All-Sky point source catalog (Skrutskie et al. 2006). However, there are 15,575 candidates with no matching information in the 2MASS database. We visually examined their spectra and identified 68 carbon stars. The  $J$ ,  $H$ , and  $J-K_s$  photometric values are available for 706,597 carbon star candidates, which are plotted in the  $J-H$  vs.  $J-K_s$  plane in Figure 2, along with the known carbon star samples. The known carbon stars

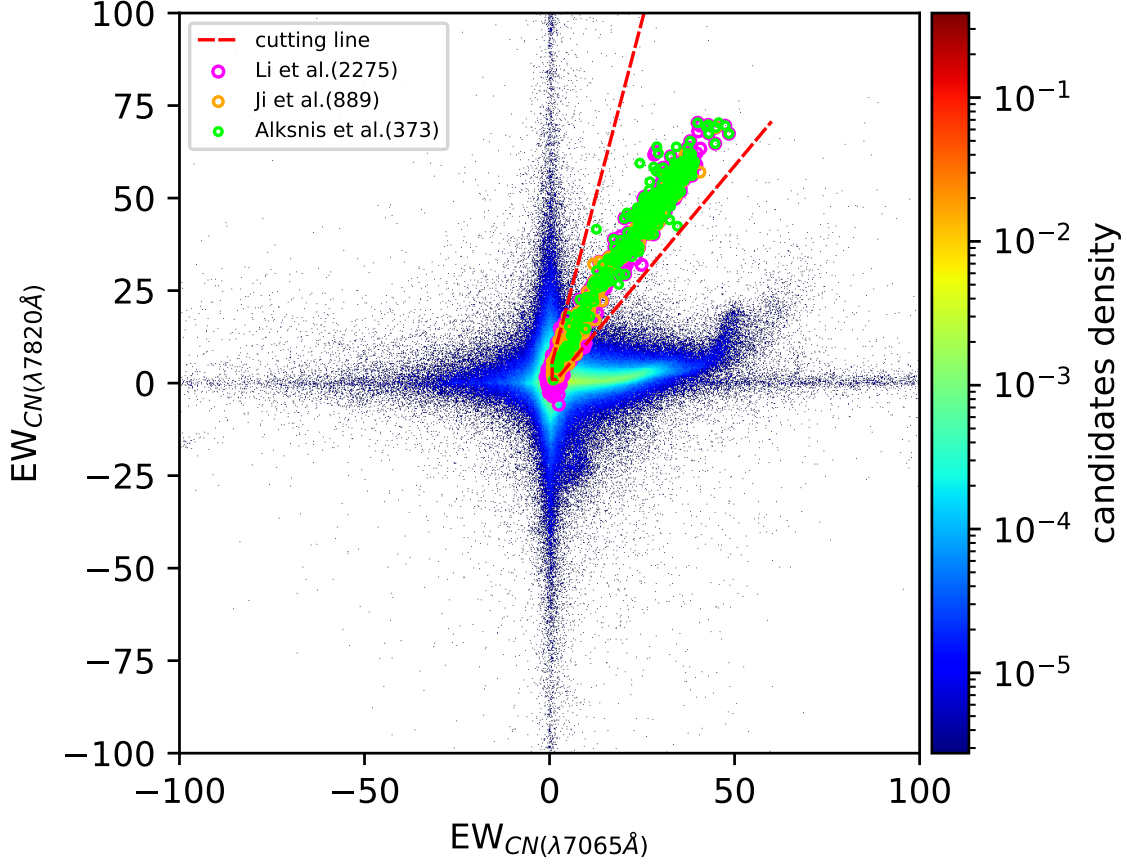


**Figure 1.** Distribution of the 9,060,920 spectra and the known carbon stars in  $EW_{CN(\lambda 7820\text{\AA})}$  vs.  $EW_{CN(\lambda 7065\text{\AA})}$  plane. The solid dots indicate the density of 9,060,920 candidates with  $S/N(i) > 10$ . The red dashed lines indicate the cuts used to remove contaminants, and the magenta, orange, and green unfilled circles represent the carbon star samples from [Li et al. \(2018\)](#), [Ji et al. \(2016\)](#), and [Alksnis et al. \(2001\)](#), respectively. The numbers in brackets indicate the number of known carbon stars in each sample.

are primarily concentrated in a narrow branch extending from the center to the upper right (see Figure 2). To remove pollution, we apply several empirical lines to simultaneously cut the candidates and known carbon star samples. The following empirical criteria are adopted.

$$\begin{aligned}
 J - H &> 0.5 \times (J - K_s) - 0.1, \\
 J - H &< 0.8 \times (J - K_s) + 0.3, \\
 J - H &> -2.0 \times (J - K_s) + 1.0.
 \end{aligned} \tag{3}$$

After applying these steps, the number of candidate samples is reduced to 609,702. Although a few known carbon stars fall outside the cutting range, the number of carbon star samples from [Alksnis et al. \(2001\)](#), [Ji et al. \(2016\)](#), and [Li et al. \(2018\)](#) is 338, 885, and 1895, respectively. Therefore, the impact of these outliers is not significant.

The strong absorption bands, such as CH ( $\lambda 4300\text{\AA}$ ) and  $C_2$  ( $\lambda 4737\text{\AA}$ ;  $\lambda 5165\text{\AA}$ ), in the blue bands, are the most obvious features of warm carbon stars (C-R, C-H, and Ba stars). On the other hand, cool carbon stars (C-N stars) show almost no flux in the blue bands. Therefore, it is important to first distinguish between warm and cool carbon candidates before using this characteristic to select carbon stars. In Figure 3 we map the candidates and known carbon stars in the  $J-H$  vs.  $H-K$  plane. The red dashed line divides them into two parts, the Warm Group on the lower left, while the Cool Group on the upper right. The equation of the red dashed line is from [Si et al. \(2015\)](#) as following

$$J - H = -0.6851 \times (H - K_s) + 1.0974. \tag{4}$$

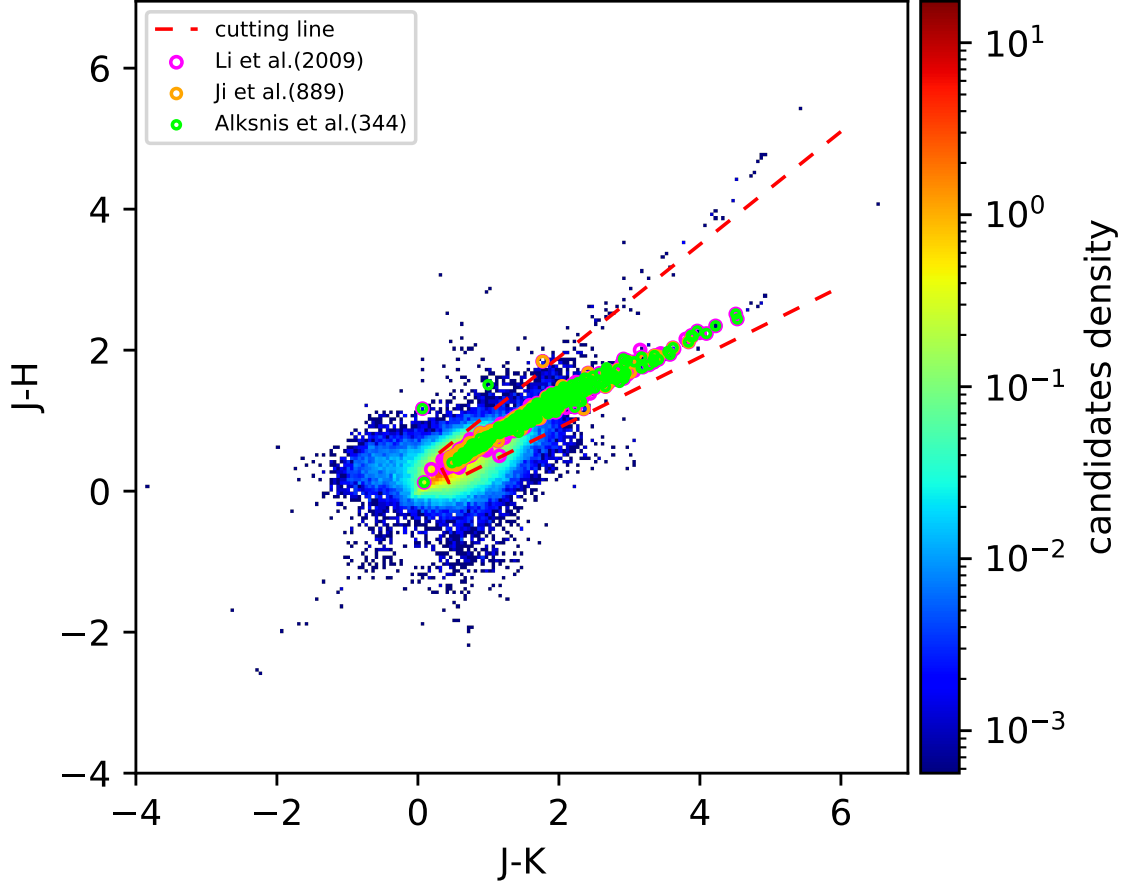


**Figure 2.** Distribution of the 706,597 candidates and the known carbon stars in the  $J-H$  vs.  $J-K_s$  color-color diagram. The solid dots indicate the density of the candidates. The other symbols are the same as in Figure 1.

### 3.1.1. The Warm Group

We present the Warm Group carbon stars in the  $EW_{C_2(\lambda 5635 \text{ \AA})}$  vs.  $EW_{C_2(\lambda 4737 \text{ \AA})}$  plane, as shown in Figure 4. We can see that the locus of the known carbon stars extends from the center of the figure to the upper right. Candidates with weak  $C_2(\lambda 4737 \text{ \AA}; \lambda 5165 \text{ \AA})$  characteristics distributed in the center region are also the major contaminants. In order to remove more contaminants, we abandoned the center region. The criteria are:

$$\begin{aligned}
 EW_{C_2(\lambda 5165 \text{ \AA})} &< 10.0 \times EW_{C_2(\lambda 4737 \text{ \AA})} + 6.0, \\
 EW_{C_2(\lambda 5165 \text{ \AA})} &> 0.3 \times EW_{C_2(\lambda 4737 \text{ \AA})} - 2.0, \\
 EW_{C_2(\lambda 5165 \text{ \AA})} &> -1.0 \times EW_{C_2(\lambda 4737 \text{ \AA})} + 6.0.
 \end{aligned} \tag{5}$$

Next, we remove as many warm star contaminants as possible in the  $EW_{C_2(\lambda 5635 \text{ \AA})}$  vs.  $EW_{CN(\lambda 7065 \text{ \AA})}$  plane. As can be seen in Figure 5, most of the known carbon stars are distributed in the upper right. In order to ensure that we can identify carbon stars visually, we use the empirical Equation (6) to remove contaminants. After this cut, 85,405 (about 67%) candidates are left. Finally, we visually identify 3631 spectra of 2903 carbon stars from the remaining 85,405 candidates.

$$\begin{aligned}
 EW_{CN(\lambda 7065 \text{ \AA})} &< 1.2, \\
 EW_{C_2(\lambda 5635 \text{ \AA})} &< 3.0.
 \end{aligned} \tag{6}$$

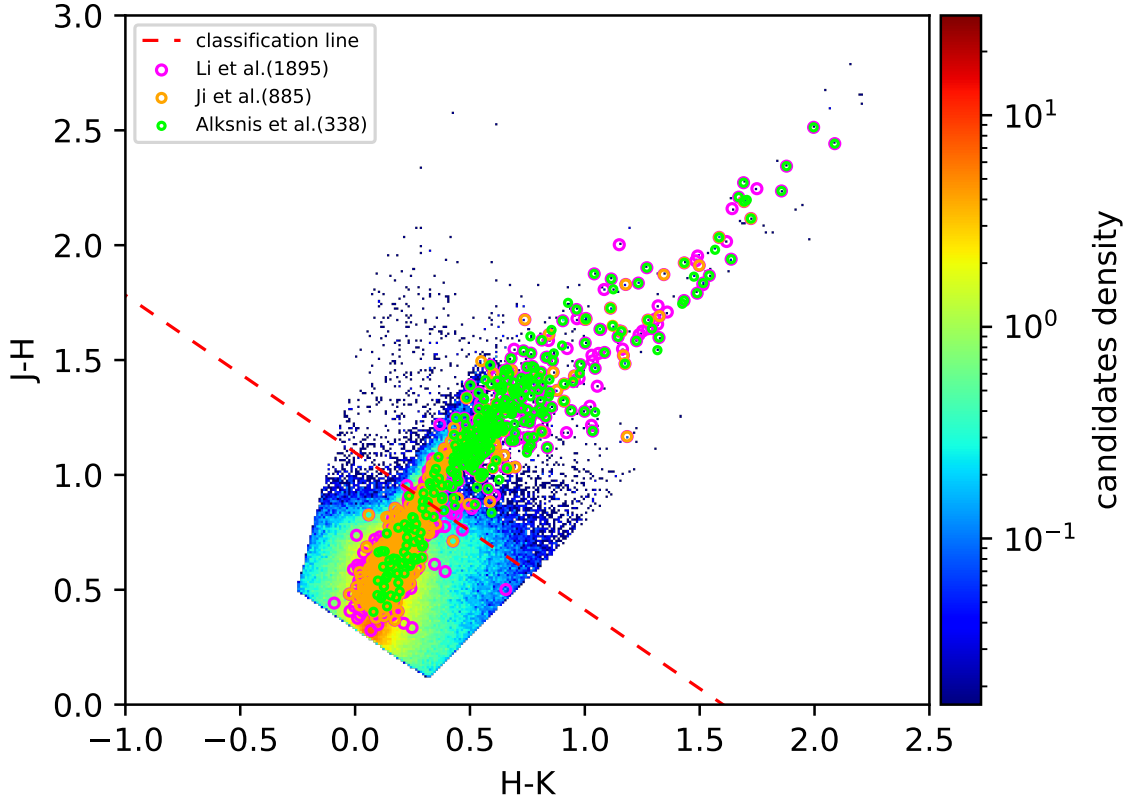


**Figure 3.** Distribution of the 609,702 candidates and the known carbon stars in the  $J - H$  vs.  $H - K_s$  color-color diagram. The solid dots with marked density represent the candidates. The red dashed line (i.e., Equation(4)) divides the candidates and known carbon stars into two groups, the Warm Group and the Cool Group. The lower left of the dashed line is the Warm Group, while the upper right is the Cool Group. The other symbols are the same as in Figure 1.

### 3.1.2. The Cool Group

The Cool Group carbon stars generally have lower temperatures, and almost all carbon stars in this group are C–N stars. Although these cool carbon stars have almost no flux at the blue end (at  $\lambda < 4400 \text{ \AA}$ , even at  $\lambda < 5000 \text{ \AA}$ ), they show strong CN absorption in the red bands. As a result, we use the  $C_2(\lambda 5635 \text{ \AA})$  and  $CN(\lambda 7820 \text{ \AA})$  molecule lines at the red end to remove contaminants. We display this group, which includes the 23,629 candidates and the known carbon star samples, in the  $EW_{C_2(\lambda 5635 \text{ \AA})}$  vs  $EW_{CN(\lambda 7820 \text{ \AA})}$  plane. As shown in Figure 6, all the known carbon stars are located in the region where  $EW_{CN(\lambda 7820 \text{ \AA})}$  is larger than a certain value, so we use Equation (7) to remove contaminants.

$$EW_{CN(\lambda 7820 \text{ \AA})} > 4.8. \quad (7)$$

After this cut, 18,325 (about 77.6%) contaminants are removed. Finally, 769 spectra of 575 carbon stars are identified by eye inspection from the remaining 5304 candidates.

### 3.2. Spectral classification

For the spectral classification of carbon stars in this work, we adopt the latest carbon star classification system published by Barnbaum et al. (1996) which divides carbon stars into mainly five types: C–R, C–H, C–N, C–J, and Ba stars. Since the isotope ratio  $^{12}C/^{13}C$  cannot be derived from the low-resolution spectrum, we cannot identify the C–J stars.

To classify the spectra of carbon stars into different sub-types, we need to understand the spectral characteristics of each sub-type, which are summarized by Si et al. (2015), Ji et al. (2016), and Li et al. (2018):



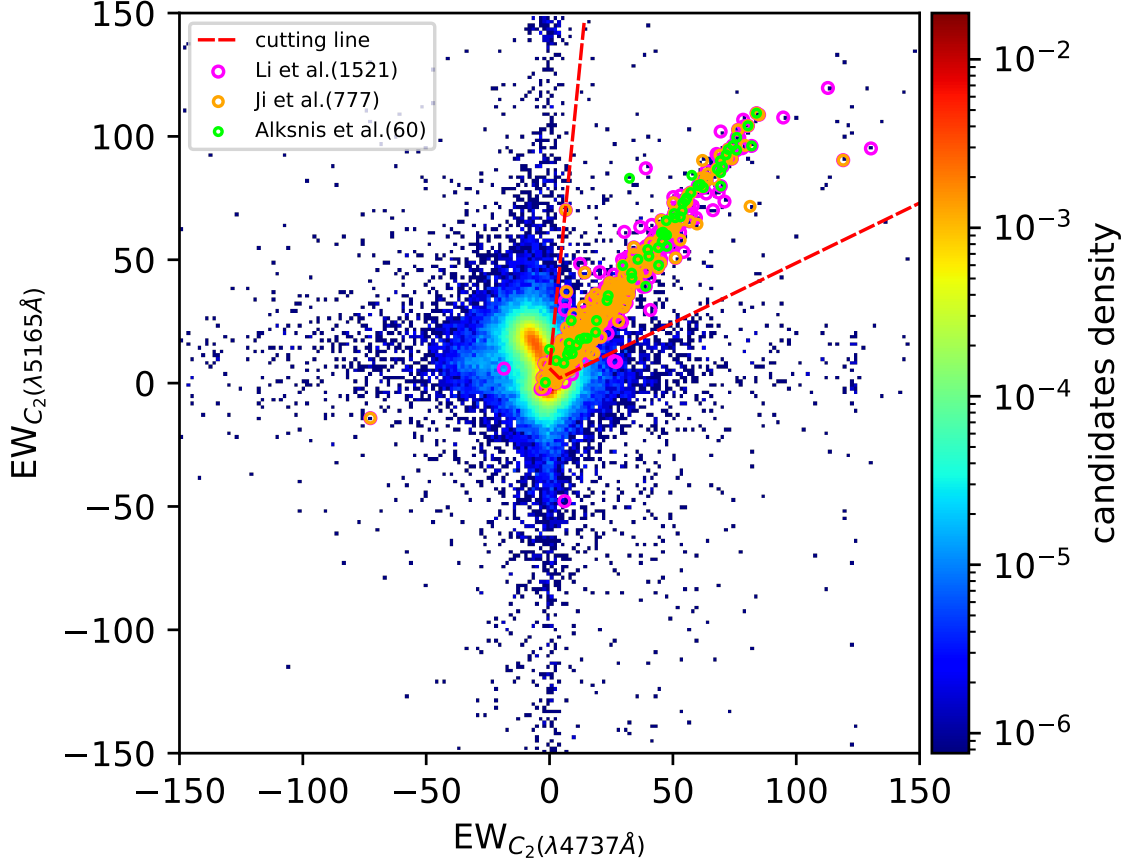


**Figure 4.** Distribution of the 586,073 warm candidates and the known carbon stars in the  $EW_{C_2(\lambda 5165\text{\AA})}$  vs.  $EW_{C_2(\lambda 4737\text{\AA})}$ . The solid dots indicate the density of the warm candidates, the red dashed lines represent the cutting lines (i.e., Equation (5)), and other symbols are the same as in Figure 1.

1. C–H stars: There is a strong G-band at  $\lambda 4300\text{\AA}$ . The secondary P-branch head near  $\lambda 4342\text{\AA}$  is the most significant feature, and the Fe I line at  $\lambda 4383\text{\AA}$  is weak, they can be used to distinguish C–H stars from C–R and Ba stars. The Ba II lines at  $\lambda 4554\text{\AA}$  and  $\lambda 6496\text{\AA}$  are very strong.
2. C–R stars: Like the strong absorption CN band at  $\lambda 4215\text{\AA}$ , the strong Ca I line at  $\lambda 4226\text{\AA}$  is also a significant feature of C–R stars. The Ba II lines at  $\lambda 4554\text{\AA}$  and  $\lambda 6496\text{\AA}$  are very weak.
3. C–N stars: There is almost no flux at  $\lambda < 4400\text{\AA}$  or even  $\lambda < 5000\text{\AA}$  which is an important feature to distinguish C–N stars from C–H and C–R stars. The isotopic bands are consistently weak, while lines of s-process elements, particularly Ba, are more enhanced than those in C–R stars.
4. Ba stars: Because Ba stars have strong enhancement of the s-process elements, the Ba II line at  $\lambda 4554\text{\AA}$  and Sr II line at  $\lambda 4077\text{\AA}$  are very strong.

According to these characteristics, we manually classify 4542 spectra of 3546 carbon stars identified in LAMOST DR7. The classification results are shown in Table 2. Figure 7 shows four typical LAMOST spectra of carbon stars classified by us, which are C–H, C–R, C–N and Ba stars, respectively. Some important characteristic lines and carbon molecular bands are marked. Among the 3546 carbon stars, 437 are defined as “UNKNOWN”, which means that we cannot classify them by spectra, Figure 8 presents five LAMOST spectra of them, and it is obvious that they are carbon stars. However, their molecular band characteristics are fuzzy, and we cannot classify them.

### 3.3. Identification results

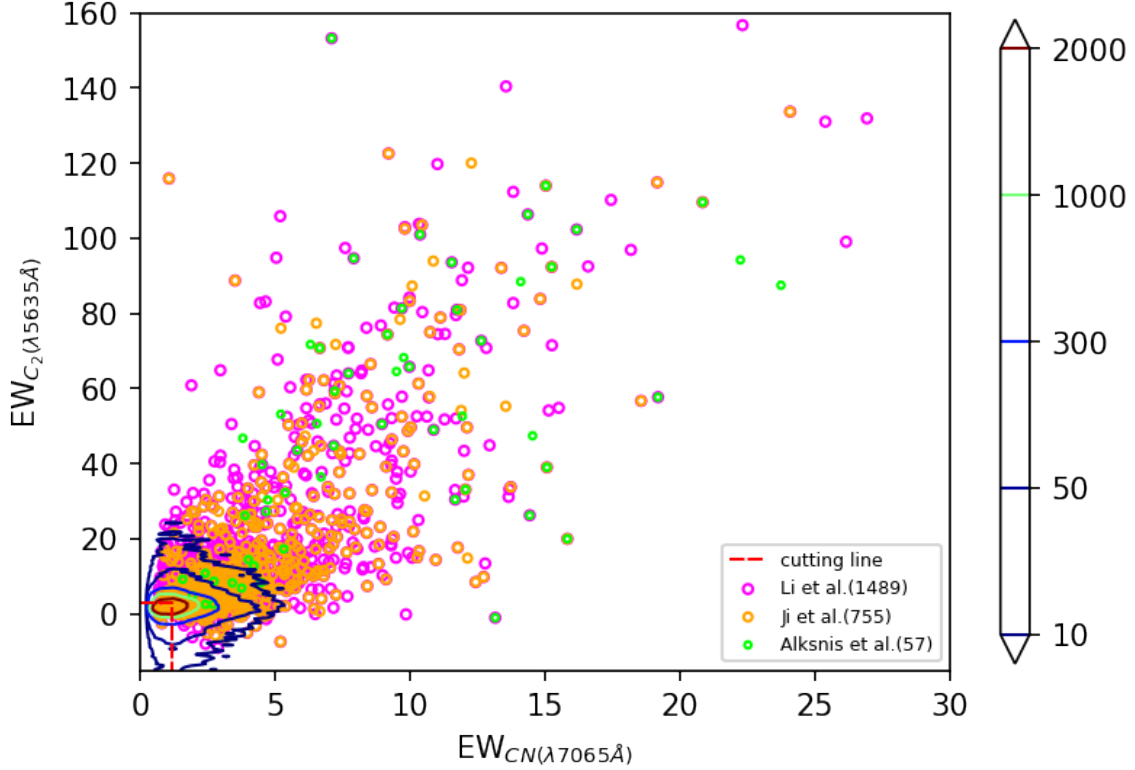


**Figure 5.** Distribution of the 127,943 warm candidates and the known carbon stars in the  $EW_{C_2(\lambda 5635\text{\AA})}$  vs.  $EW_{CN(\lambda 7065\text{\AA})}$  plane. The contours represent the density of the candidates. The red dashed lines are the cutting lines (i.e., Equation (6)). Other symbols are the same as in Figure 1.

**Table 2.** Carbon Stars in This Work

Subtype	Number of Carbon Stars	Number of Carbon Stars Spectra
C-H	925	1217
C-R	284	341
C-N	608	799
Ba	1292	1657
UNKNOWN	437	528
Total Number	3546	4542

By searching for the warm group and the cool group, we identified 2903 carbon stars belonging to the hot group, while 575 carbon stars belonged to the cool group. Additionally, we identified 68 carbon stars in the candidates with no matching information in the 2MASS database. The specific identification steps are summarized in Figure 9, and the final result is presented in Table 2. The information of some example carbon stars is shown in Table 3.

#### 4. DISCUSSION

##### 4.1. Compare with the identification results of LAMOST DR7 pipeline and LAMOST DR4 catalog



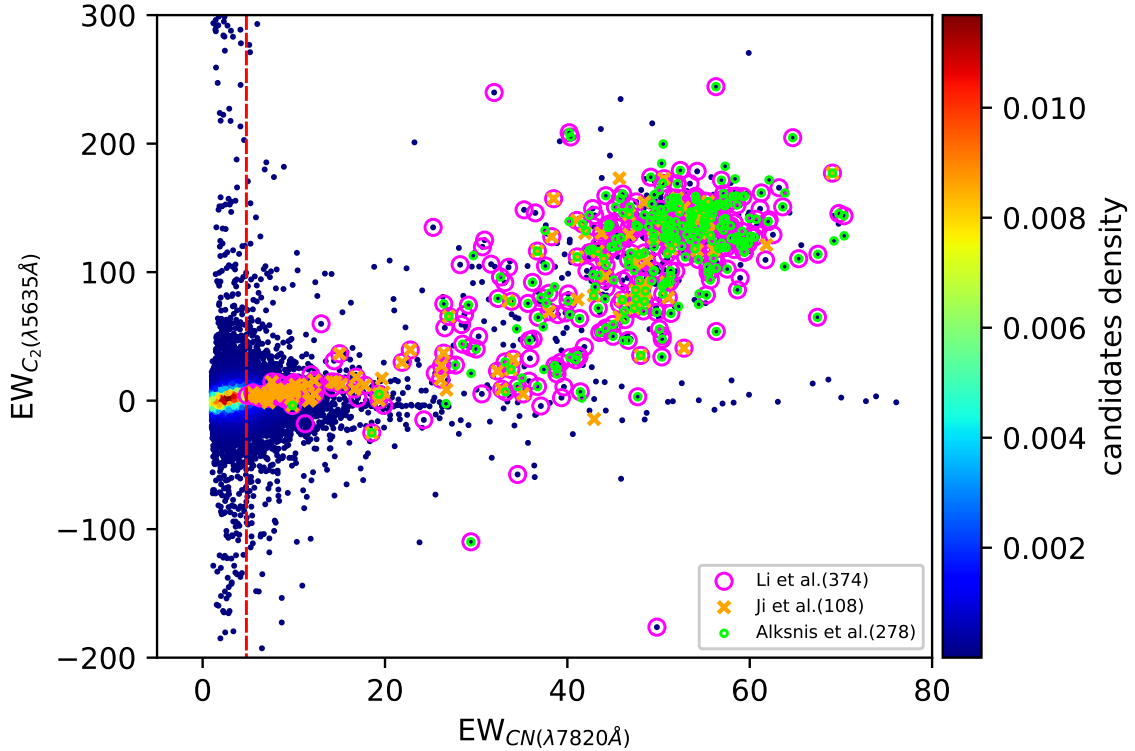


**Figure 6.** The distribution of 23,629 cool candidates and known carbon stars in the  $EW_{C_2(\lambda 5635\text{\AA})}$  vs.  $EW_{CN(\lambda 7820\text{\AA})}$  plane. The red dashed line represents the cutting line (i.e., Equation (7)). The dots indicate the density of the candidates. The other symbols are the same as in Figure 1.

**Table 3.** Carbon Stars Discovered in LAMOST DR7

obsid	designation	ra (degree)	dec (degree)	subclass <sup>a</sup>	$M_G$ (mag)	$(G_{BP}-G_{RP})_0$ (mag)	sp_type <sup>b</sup>	dwarf <sup>d</sup>
492105114	J000021.94+251921.8	0.09115	25.322726	Carbon	0.106571964	1.111763218	C-H	0
182607108	J000043.94+463317.7	0.183084	46.554929	Carbon	1.387818663	1.16221294	Ba	0
269401237	J000043.99+544642.3	0.183294	54.778429	Carbon	-0.541169969	1.29267988	Ba	0
248409244	J012137.11+513725.5	20.404644	51.623759	Carbon	-2.167650566	2.586834633	C-N	0
368508222	J012150.43+011301.3	20.4601405	1.217029	Carbon	9.61557705	1.783483731	C-N	1
407815063	J012153.97+411341.2	20.474905	41.228134	Carbon	1.209880871	1.260210652	Ba	0
470104224	J012300.73+190749.0	20.75305	19.1302973	Carbon	4.082624671	1.035243017	C-R	0
393004088	J012302.65+465155.3	20.761044	46.865362	G5	-0.707715317	1.48405494	Ba	0
69216250	J004637.24+401824.8	11.655199	40.306906	Carbon	8.980534815	1.803201731	UNKNOWN <sup>c</sup>	1

<sup>a</sup>Spectral sub-type given by LAMOST DR7 pipeline

<sup>b</sup>Spectral sub-type.

<sup>c</sup>Carbon stars with no identifiable sub-type.

<sup>d</sup>1 means that the carbon star is a dwarf, while 0 for a giant.

In the LAMOST DR7 LRS General Catalog, there are 3565 stars (4420 spectra) have been marked as “carbon”. Firstly, 84.24% of our carbon stars have been correctly classified as carbon stars by the LAMOST DR7 pipeline, and the other 15.76% (559) are only recognized by our method. Among these incorrectly classified carbon stars, 95.53% (534) have been classified as G5-type stars, and others have been categorized as K5-type star (one), K4-type star (six), K1-type stars (one), and unknown (17), respectively. In our carbon catalog, these stars are classified as 520 Ba, 13 C-N, 12 C-H, 10 C-R, and 4 UNKNOWN, respectively.

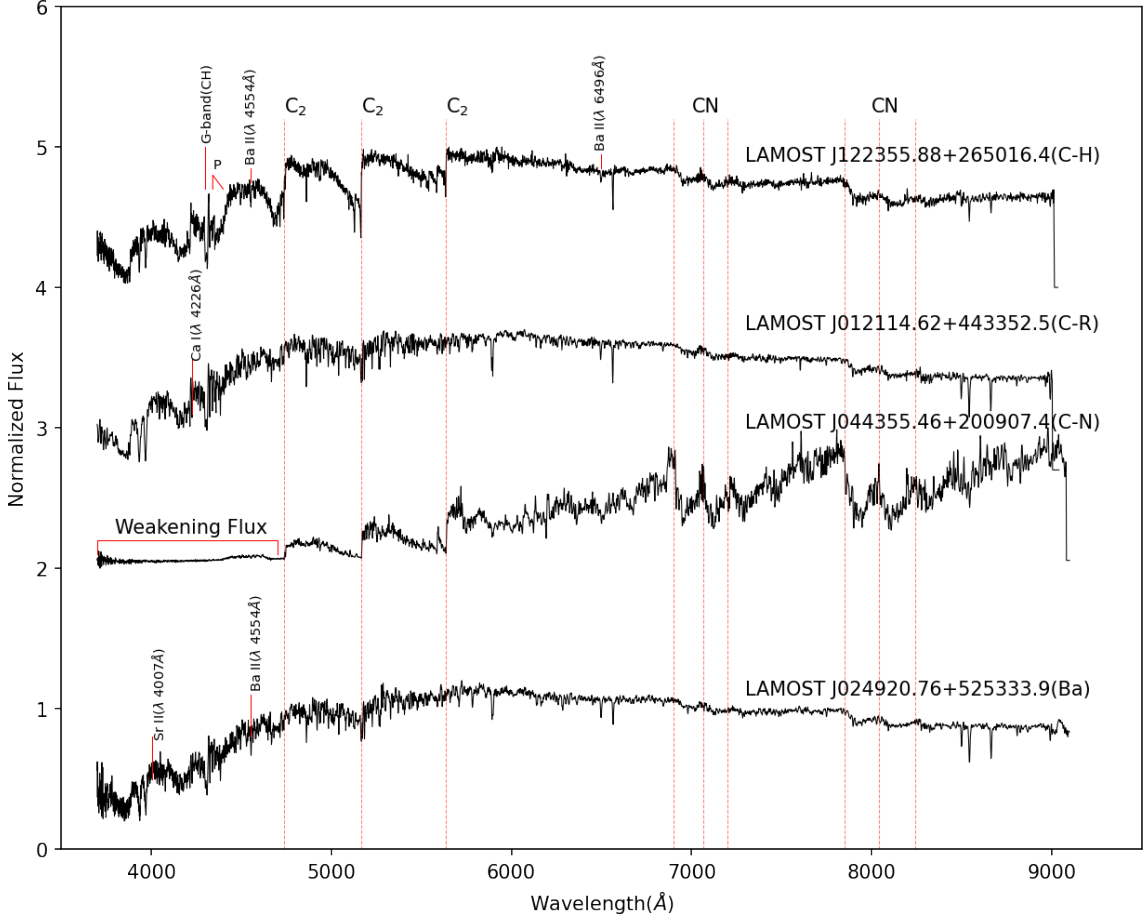


**Figure 7.** The normalized spectra of four LAMOST carbon stars come from this work, including a C–H star, a C–R star, a C–N star and a Ba star. The G-branch, P-branch band, and Ba II lines are marked for the C–H star by red color. For the spectrum of a C–R star, we label the Ca I line. The weakening flux in the C–N spectrum is labeled in the blue part. The Ba II and Sr II lines are also marked by red color for the Ba star. The red dashed lines represent C<sub>2</sub> bands in the blue part and CN bands in the red part.

Then we checked the stars (578) that were marked as “carbon” by the LAMOST DR7 pipeline but not by us, using our identification steps in Section 3. Most of them (81%) were removed by Equation (2), since they have relatively weak CN(7280 Å) and CN(7065 Å) line. The remaining 19% have  $J$ ,  $H$ , and  $J-K_s$  photometric, while they all have small line index, and generally fall close to (0,0) in the line index planes, therefore they are discarded when cutting carbon star candidates. We visually inspected these stars, 567 of them are confirmed as true carbon stars, as shown in Table 4. About half of them (279) are classified as C–H stars, while, there are 77, 46, 33, and 132 stars categorized as Ba, C–N, C–R stars, and “UNKNOWN”, respectively. The S/Ns are very low for the remaining 11 stars, so it’s not sure if they are carbon stars.

Comparing with LAMOST DR4 carbon star catalog of (Li et al. 2018), we find that there are 764 stars included in the LAMOST DR4 catalog, while they are not contained in (Li et al. 2018). There are 537 stars included in Li et al. (2018), while we have not found. The reason is that those stars have weak CN bands, therefore, we have omitted them as discussed in Section 3. Among these stars, 249 objects have also been also identified as carbon stars by the LAMOST DR7 pipeline.

Because we can not know definitively the number of carbon stars in the massive LAMOST DR7 data set, it is impossible to accurately estimate the completeness and contamination rates of our method. However, we can roughly evaluate the upper limit of completeness as  $3546/(3546 + 567) \approx 86.21\%$ . Since the carbon stars in our work were visually confirmed, the contamination rate is very low.

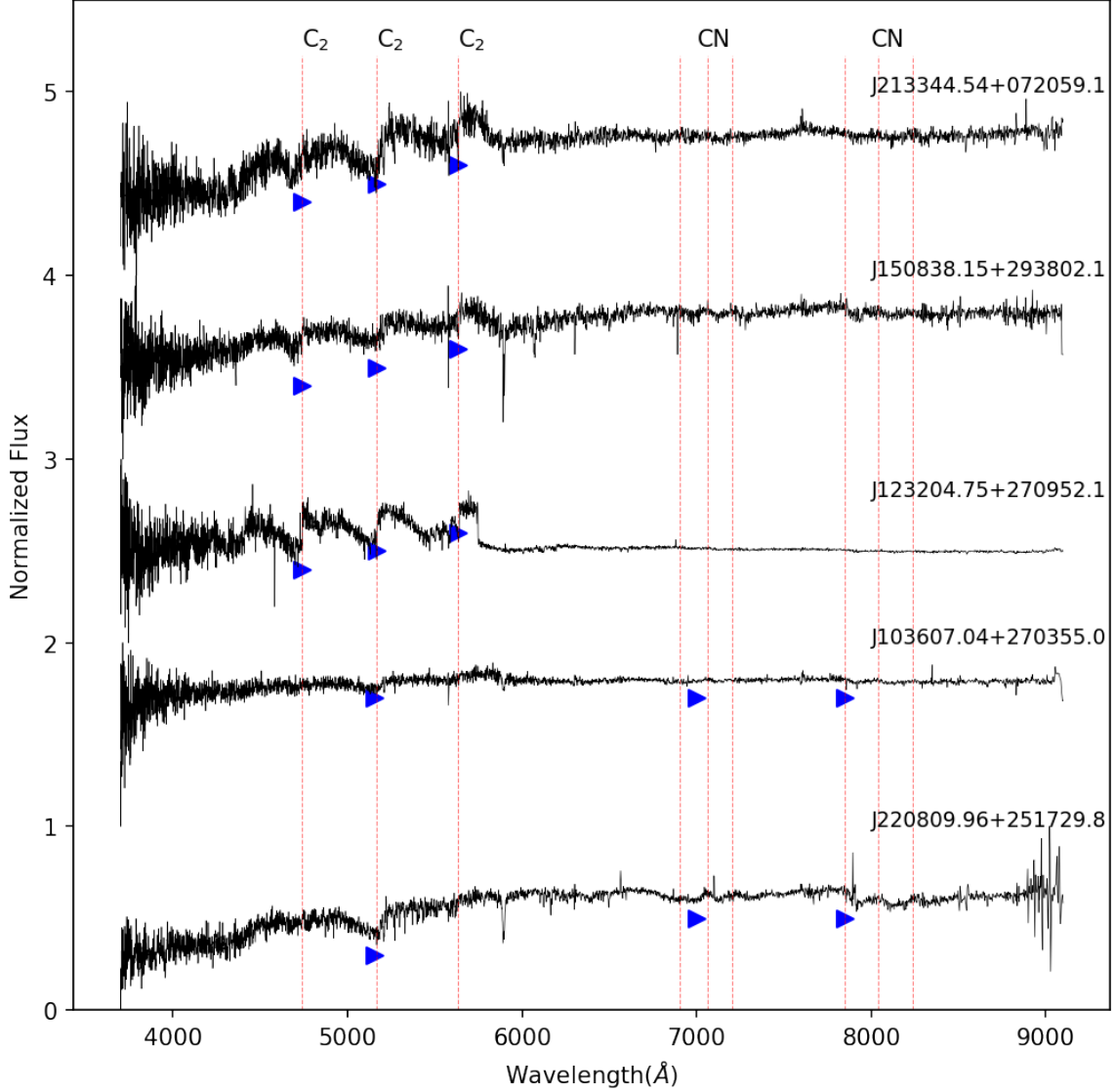


**Figure 8.** Normalized LAMOST spectra of five carbon stars classified as “UNKNOWN”. The red dashed lines represent the C2 bands in the blue part and CN bands in the red part. The blue triangles represent the carbon features we are using to call these carbon stars.

**Table 4.** Sub-type of Carbon Stars Marked as ”carbon” by LAMOST DR7 Pipeline

obsid	designation	ra (degree)	dec (degree)	sp_type
616307219	J031910.17+620020.8	49.792375	62.005787	C-N
645002216	J124804.83+594334.1	192.0201253	59.7261532	C-H
199404230	J060920.95+593107.1	92.337312	59.518646	Ba
617401149	J011427.00+590944.1	18.612503	59.162267	C-H
157909037	J040030.35+584828.8	60.126463	58.808008	Ba
583213247	J133536.72+574224.0	203.900881	57.706683	C-H
32208015	J115227.75+571342.9	178.115656	57.228607	UNKNOWN

#### 4.2. Distribution of our carbon stars in the $J-H$ vs. $H - K_s$ diagram

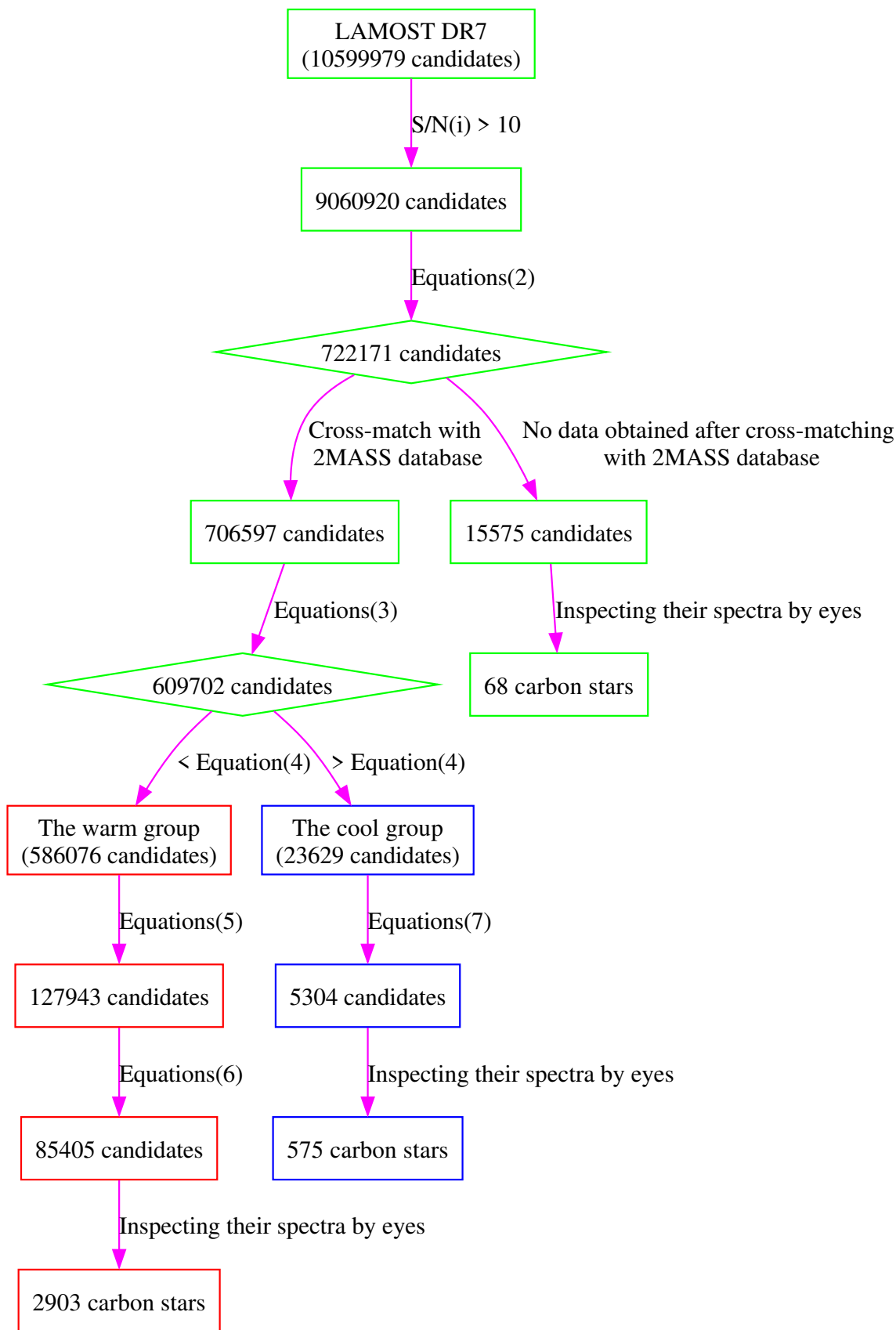


**Figure 9.** Steps of carbon stars identification.

$JHK_s$  colors are a good indicator of effective temperature (Wang & Jiang 2014), therefore, they are often used to distinguish sub-type carbon stars with different temperatures. Totten et al. (2000) used the  $J - H$  vs.  $H - K_s$  two-color diagram to distinguish C–N stars from C–H stars, and determined the approximate location of dC stars. Gigoyan et al. (2012) showed the distribution of C–H stars and C–N stars on the  $J - H$  vs.  $H - K$  two-color diagram. Si et al. (2015) also analyzed the distribution positions of different types of carbon stars on the  $J - H$  vs.  $H - K_s$  two-color diagram, and provided the dividing line between C–H stars and C–N stars (i.e., Equation(4)).

The carbon stars classified in this work are mapped in the  $J - H$  vs.  $H - K_s$  plane in Figure 10, and the magnitudes of  $JHK_s$  come from the 2MASS database (Skrutskie et al. 2006). It can be seen that, in Figure 10, the black straight line (Equation (4)) can separate C–H, C–R and Ba stars from C–N stars well. After statistics, the accuracy of Equation (4) to distinguish C–N from C–H, C–R and Ba stars are 99.9%, 100%, 99.2%, respectively. There are only three C–N stars that fall on the lower left of the black solid line. We check the flag “QH” of these stars in the 2MASS catalog, which indicates the quality of the photometry in each band. It shows that except for the  $K_s$  band of, “J055802.69+282737.4”, all the rest bands have the best quality detections, with measurement uncertainties smaller than 0.15 mag. Thus, Equation (4) can select the C–N stars with the completeness of 98.9% and a contamination rate of only 4.3%, therefore, it can be used as a relatively reliable dividing line between C–N stars and the other three sub-types.

#### 4.3. Identification of carbon dwarfs

Dwarf carbon (dC) stars are main-sequence stars that show molecular absorption bands of carbon. In the mass-transfer binary (MTB), the dC progenitor accreted carbon-enhanced stellar wind material from a more massive companion that evolved into a thermally-pulsing AGB (TP-AGB) star. The dC progenitor now bears the atmospheric traces of carbon as a dC star. The TP-AGB expelled its envelope via the wind, leaving behind a white dwarf (WD), and it is now usually beyond detection in optical spectra. Previous works have shown that many carbon stars are actually carbon dwarf stars (Green 2013; Green et al. 2019; Roulston et al. 2022). We can easily distinguish carbon dwarfs and giants in the H-R diagram. In Figure 11, we show the H-R diagram constructed by  $G_{BP}-G_{RP}$  and the absolute magnitude  $M_G$  of our 3482 carbon stars. We obtain the broad-band (G), the  $G_{BP}-G_{RP}$  magnitude from Gaia DR3 (Gaia Collaboration et al. 2021) and distances from Bailer-Jones et al. (2021). The extinction and reddening in  $G$  and  $G_{BP}-G_{RP}$  are corrected by adopting the  $E(B - V)$  values of Green et al. (2019) and extinction coefficient of Wang & Chen (2019).

The 606 dC stars identified by Green (2013) are also presented in Figure 11, and it can be seen that the known dC stars, shown by the grey dots, are distributed in the main sequence. Then we choose a screening condition, with  $M_G > 5.0$  mag (Roulston et al. 2022), to select dC stars. The black dashed line in Figure 11 represents the dividing line between carbon dwarfs and carbon giants. The lower part represents the distribution area of carbon dwarfs, while the upper part is for the carbon giants. We note that there is a C–N star “J101525.92-020431.8”, in the lower area. We search for it in the SIMBAD astronomical database<sup>2</sup>, and find that it is classified by Maunon et al. (2004) as an AGB type carbon star in the halo. Therefore, we exclude it as a dC candidate.

Finally, we identify 258 carbon dwarf stars, including 33 Ba, 104 C–H, 21 C–R and 100 “UNKNOWN” stars. We note that there is a large number of dCs belong to C–H stars. This is probably because, like dCs, C–H stars are also thought to be post MTB given their orbital properties (Izzard et al. 2010). They have suffered wind accretion from a former AGB companion, which is now a white dwarf. The number of dC stars classified as “UNKNOWN” stars is relatively larger, and the fraction of “UNKNOWN” for dwarfs is 40%, it is much higher than 10% for giants. This result might be explained by the fact that the low luminosity of dC stars leads to the low S/Ns of their observed spectra, thus, we cannot subclassify them. Since the character lines we used to classify carbon stars are mainly in the  $g$ -band of the LAMOST spectra, we show the distribution of S/Ns in  $g$ -band in Figure 12. As expected, the S/Ns of dCs and “UNKNOWN” stars are statistically much lower than those of carbon giants and classified carbon stars, respectively.

#### 4.4. Spatial Distribution

The spatial distribution in Galactic coordinates of the 3546 carbon stars is plotted in Figure 13. Among them, 4.6% C–N, 63.1% C–H, 28.2% C–R and 16.3% barium stars are located in the regions with  $|b| \geq 30^\circ$ . As expected, the

<sup>2</sup> <http://simbad.u-strasbg.fr/simbad/>

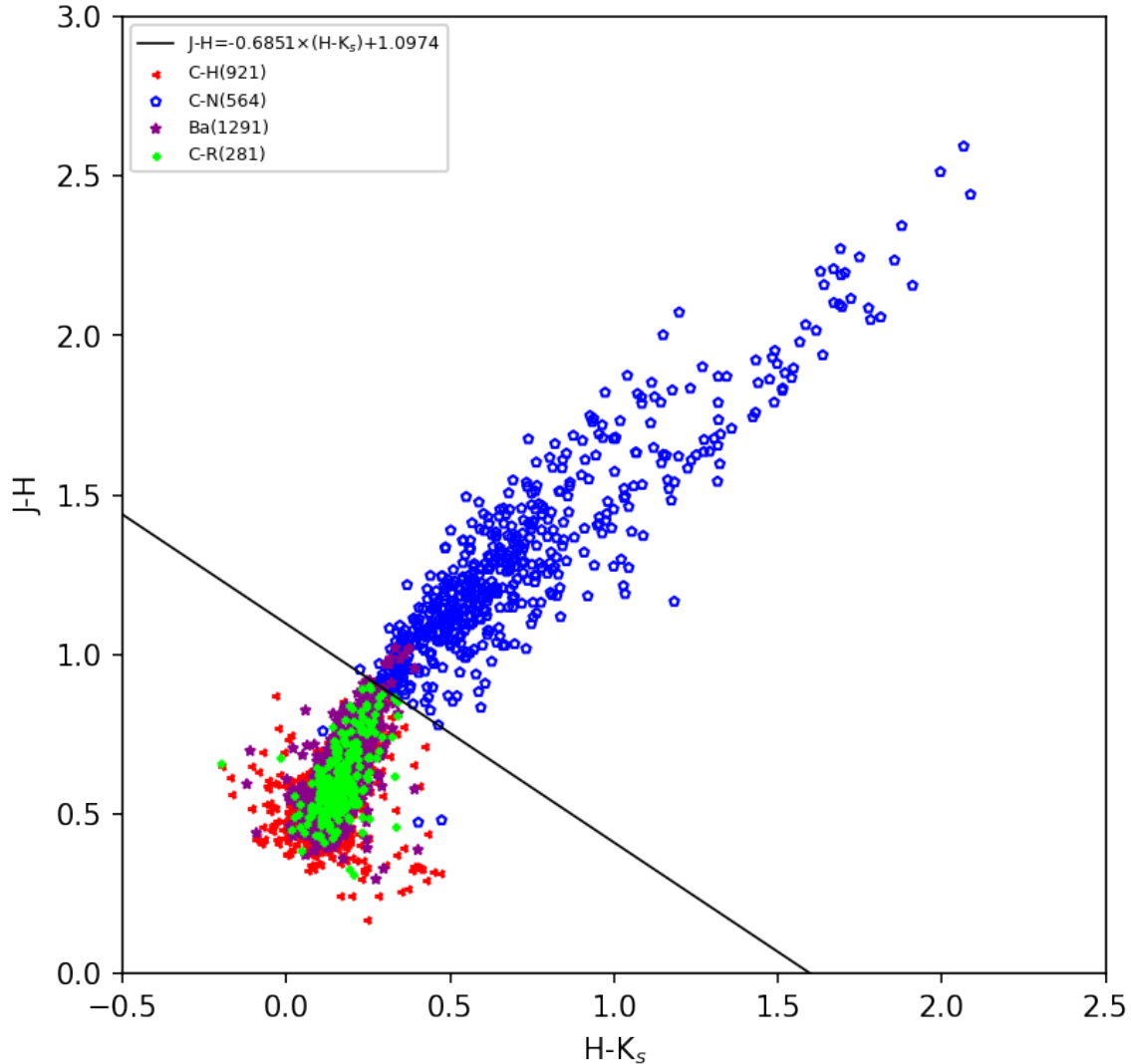


**Figure 10.** Distribution of our carbon stars in the  $J - H$  vs.  $H - K_s$  diagram. The black solid line (see Equation (4)) is the dividing line between the warm carbon stars (C–H, C–R, Ba stars) and the cool carbon stars (C–N stars). The blue unfilled pentagon symbols represent the C–N stars, the red dendritic symbols toward the left represent the C–H stars, the dark magenta star symbols represent the Ba stars, and the green crosses display the C–R stars.

majority of C–N (95%) and a large number of C–R (72%) and barium stars (84%) are concentrated at low Galactic latitudes. A majority of the C–H stars lie in high latitudes, similar to previous works (Ji et al. 2016; Li et al. 2018), since C–H stars are found mostly in halo populations (Goswami 2005; Goswami et al. 2010) of the Galaxy. Among the 437 “UNKNOWN” stars, 179 locate at  $|b| \geq 30^\circ$ , account for about 40%. Most of the dC stars (70.9%) distribute at high Galactic latitudes, which supports that dC stars are from the older thick-disk and halo populations (Farihi et al. 2018; Roulston et al. 2022)

## 5. CONCLUSION

In this work, we use the multiple line index planes, 2MASS near-infrared color-color diagrams and manual inspections to identify carbon stars. We have carried out eye inspection and classification of the selected carbon star candidates one by one, therefore, the carbon star samples we finally obtained have the characteristics of high purity and good consistency. However, we lose the candidates with a small line index when cutting carbon star candidates, and they generally fall close to (0,0) in the online index plane. Compared with the identification results by the pipeline for the

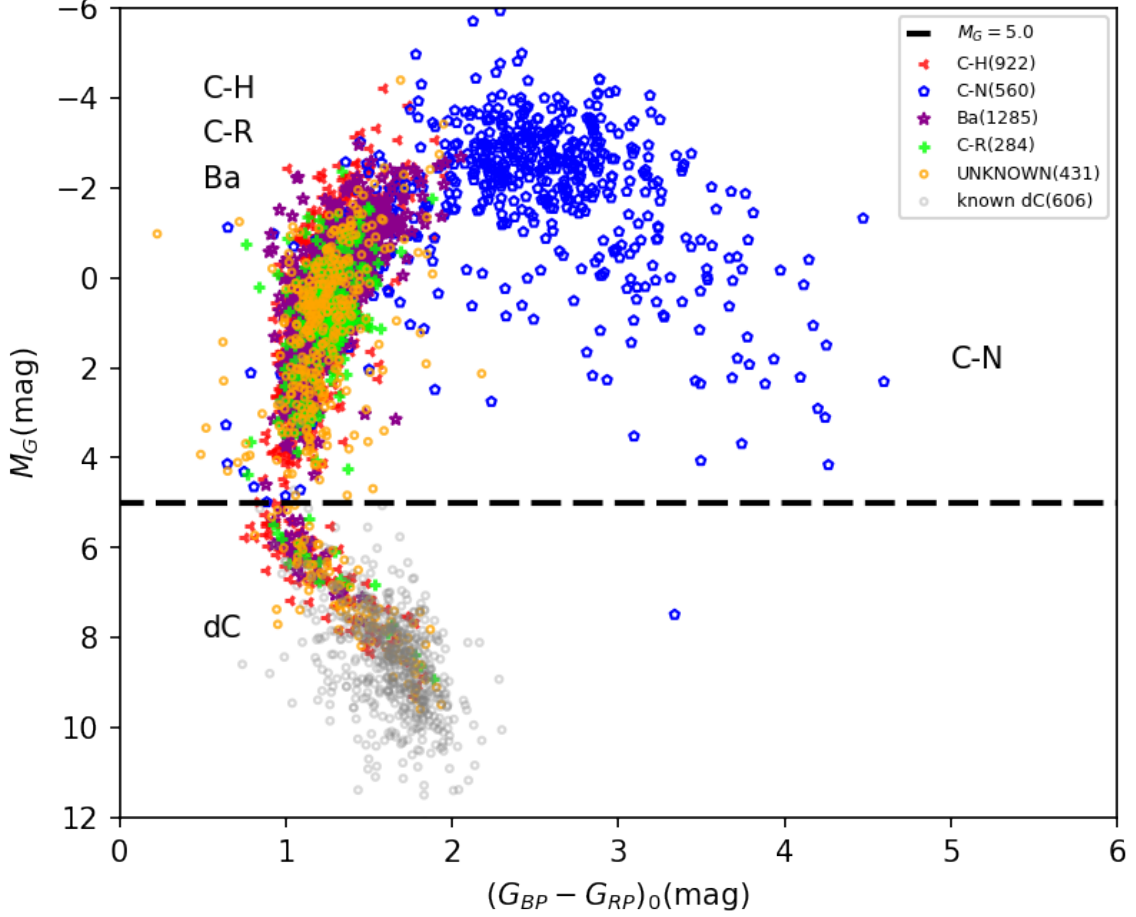


**Figure 11.** Distribution of our carbon stars in the H-R diagram. The black dashed line represents the dividing line between carbon dwarfs and carbon giants (i.e.,  $M_G=5.0$  mag). The orange and gray circles represent “UNKNOWN” stars and dC stars identified by Green (2013), respectively. The other symbols are the same as in Figure 10. The numbers in parentheses indicate the quantities of each sub-type.

LAMOST DR7 spectra and those from LAMOST DR4 by Li et al. (2018), 559 and 1432 carbon stars, respectively, are unique in our catalog.

We have identified 3546 carbon stars (4542 spectra) from the low-resolution spectra of more than 10 million in LAMOST DR7 including 925 C-H, 1392 Ba, 608 C-N and 284 C-R stars. We have labeled 437 unclassified carbon stars as “UNKNOWN”. In the  $J - H$  vs.  $H - K_s$  two-color diagram, the Equation (4) can be used as a relatively reliable dividing line between C-N stars and other three sub-types.

Through mapping our carbon star candidates in the H-R diagram, we have identified 258 dC star candidates from 3546 carbon stars, including 33 Ba, 104 C-H, 21 C-R, and 100 “UNKNOWN” stars.

We discussed the spatial distribution of each sub-type carbon star in the Milky Way. Most of our carbon stars are distributed in the anti-galactic direction, which is caused by the LAMOST’s sky survey strategy. The spatial distribution confirms that C-H stars are mostly found in halo populations. As expected, the majority of C-N, C-R, and Ba stars are distributed at low Galactic latitudes. Among the 437 “UNKNOWN” stars, 179 located at  $|b| \geq 30^\circ$ , account for about 40%.

It would be very helpful for performing follow-up time domain photometric and high-resolution spectroscopic observations in the future in order to identify more carbon stars and further investigate their nature.



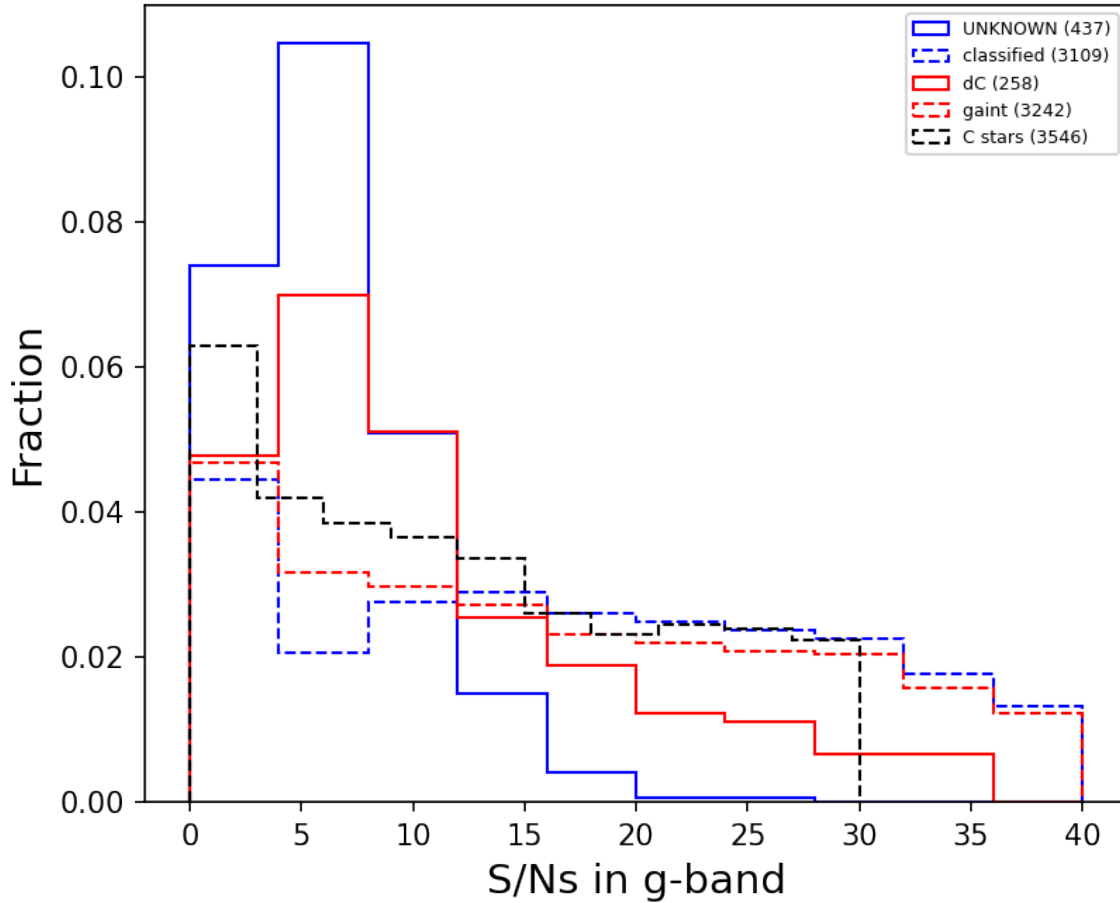


**Figure 12.** Distribution of S/Ns in LAMOST  $g$ -band. The blue solid and dashed lines represent the “UNKNOWN” and classified carbon stars, respectively. The red solid and dashed lines represent the dCs and carbon giants, respectively. The S/N distribution of all the carbon stars is also shown by the black dashed line.

We thank Shuai Feng for useful discussions. This study is supported by the National Natural Science Foundation of China under grants Nos. 11903012, 12173013, 11803006, 12090040, 12090044, 11833006, 12203016; the Hebei NSF No. A2019205166, A2021205006, 226Z7604G, A2022205018. We acknowledge the science research grants from the China Manned Space Project with No. CMS-CSST-2021-A09; Science and Technology Project of Hebei Education Department. The Guoshoujing Telescope (the Large Sky Area Multi-Object Fiber Spectroscopic Telescope LAMOST) is a National Major Scientific Project built by the Chinese Academy of Sciences. LAMOST is operated and managed by the National Astronomical Observatories, Chinese Academy of Sciences.

## REFERENCES

- Abate, C., Stancliffe, R. J., & Liu, Z.-W. 2016, *A&A*, 587, A50, doi: [10.1051/0004-6361/201527864](https://doi.org/10.1051/0004-6361/201527864)
- Aikman, G. C. L. & McClure, R. D. 1984, *JRASC*, 78, 205
- Alksnis, A., Balkavs, A., Dzervitis, U., et al. 2001, *BaltA*, 10, 1, doi: [10.1515/astro-2001-1-202](https://doi.org/10.1515/astro-2001-1-202)
- Bailer-Jones, C. A. L., Rybizki, J., Fouesneau, M., Demleitner, M., & Andrae, R. 2021, *VizieR Online Data Catalog*, I/352
- Duchêne, G. & Kraus, A. 2013, *ARA&A*, 51, 269, doi: [10.1146/annurev-astro-081710-102602](https://doi.org/10.1146/annurev-astro-081710-102602)
- Barnbaum, C., Stone, R. P. S., & Keenan, P. C. 1996, *ApJS*, 105, 419, doi: [10.1086/192323](https://doi.org/10.1086/192323)
- Battinelli, P., Demers, S., Rossi, C., & Gigoyan, K. S. 2013, *Appl. Phys.*, 56, 68, doi: [10.1007/s10511-013-9268-7](https://doi.org/10.1007/s10511-013-9268-7)
- Boothroyd, A. I., & Sackmann, I. J. 1988, *ApJ*, 328, 653, doi: [10.1086/166323](https://doi.org/10.1086/166323)

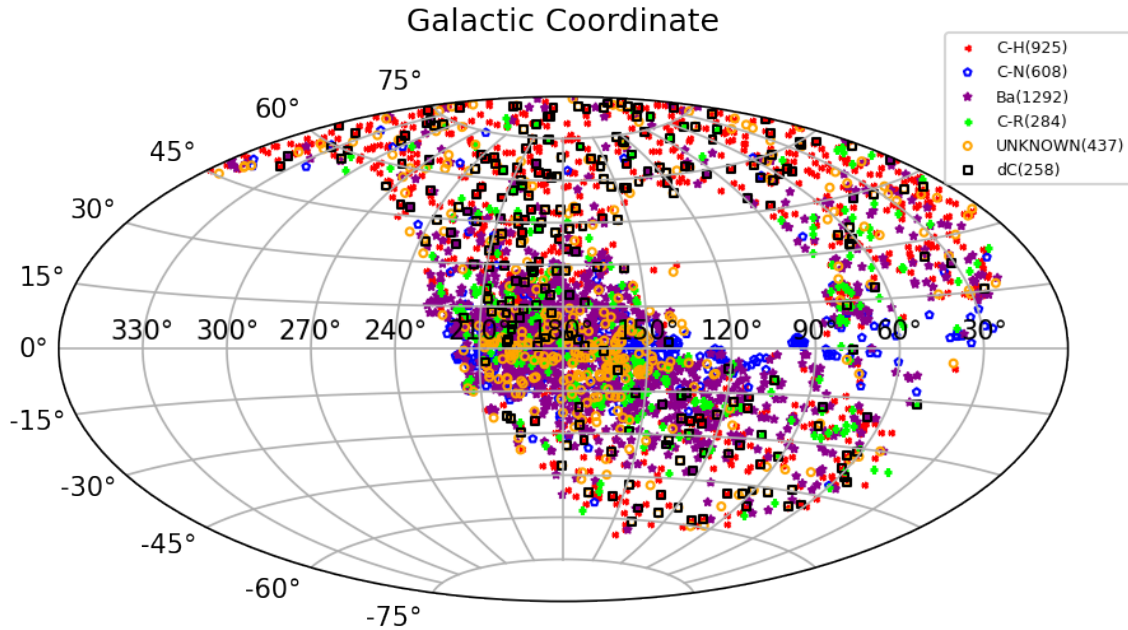


**Figure 13.** Spatial distribution of the 3546 carbon stars reported in this paper in the Galactic Coordinates. The black squares represent dC stars, the other symbols are the same as in Figure 10. The numbers in parentheses indicate the quantities of each sub-type.

- Christlieb, N., Green, P. J., Wisotzki, L., Reimers, D. 2001, *A&A*, 375, 366, doi: [10.1051/0004-6361:20010814](https://doi.org/10.1051/0004-6361:20010814)
- Cui, X. Q., Zhao, Y. H., Chu, Y. Q., et al. 2012, *Research in Astronomy and Astrophysics*, 12, 1197, doi: [10.1088/1674-4527/12/9/003](https://doi.org/10.1088/1674-4527/12/9/003)
- Dahn, C. C., Liebert, J., Kron, R. G., Spinrad, H., & Hintzen, P. M. 1977, *ApJ*, 216, 757, doi: [10.1086/155518](https://doi.org/10.1086/155518)
- Demers, S., Battinelli, P. 2007, *A&A*, 473, 143, doi: [10.1051/0004-6361:20077691](https://doi.org/10.1051/0004-6361:20077691)
- Downes, R. A., Margon, B., Anderson, S. F., et al. 2004, *AJ*, 127, 2838, doi: [10.1086/383211](https://doi.org/10.1086/383211)
- Escorza, A. & De Rosa, R. J. 2023, *A&A*, 671, A97. doi: [10.1051/0004-6361/202244782](https://doi.org/10.1051/0004-6361/202244782)
- Farihi, J., Arendt, A. R., Machado, H. S., et al. 2018, *MNRAS*, 477, 3801. doi: [10.1093/mnras/sty890](https://doi.org/10.1093/mnras/sty890)
- Gaia Collaboration, Brown, A. G. A., Vallenari, A., et al. 2021, *A&A*, 649, A1, doi: [10.1051/0004-6361/202039657](https://doi.org/10.1051/0004-6361/202039657)
- Gigoyan, K. S., Rossi, C., Sclavi, S., & Gaudenzi, S. 2012, *Appl. Phys.*, 55, 424, doi: [10.1007/s10511-012-9248-3](https://doi.org/10.1007/s10511-012-9248-3)
- Goswami, A. 2005, *MNRAS*, 359, 531, doi: [10.1111/j.1365-2966.2005.08917.x](https://doi.org/10.1111/j.1365-2966.2005.08917.x)
- Goswami, A., Karinkuzhi, D., & Shantikumar, N. S. 2010, *MNRAS*, 402, 1111. doi: [10.1111/j.1365-2966.2009.15939.x](https://doi.org/10.1111/j.1365-2966.2009.15939.x)
- Goswami, P. P. & Goswami, A. 2023, *AJ*, 165, 154. doi: [10.3847/1538-3881/aca971](https://doi.org/10.3847/1538-3881/aca971)
- Green, G. M., Schlafly, E., Zucker, C., Speagle, J. S., & Finkbeiner, D. 2019, *ApJ*, 887, 93, doi: [10.3847/1538-4357/ab5362](https://doi.org/10.3847/1538-4357/ab5362)
- Green, P. 2013, *ApJ*, 765, 12, doi: [10.1088/0004-637X/765/1/12](https://doi.org/10.1088/0004-637X/765/1/12)
- Green, P. J. 2000, *IAUS*, 177, 27
- Green, P. J., Montez, R., Mazzoni, F., et al. 2019, *ApJ*, 881, 49. doi: [10.3847/1538-4357/ab2bf4](https://doi.org/10.3847/1538-4357/ab2bf4)
- Iben, I., J., & Renzini, A. 1983, *ARA&A*, 21, 271, doi: [10.1146/annurev.aa.21.090183.001415](https://doi.org/10.1146/annurev.aa.21.090183.001415)
- Izzard, R. G., Dermine, T., & Church, R. P. 2010, *A&A*, 523, A10. doi: [10.1051/0004-6361/201015254](https://doi.org/10.1051/0004-6361/201015254)
- Ji, W., Cui, W. Y., Liu, C., et al. 2016, *ApJS*, 226, 1, doi: [10.3847/0067-0049/226/1/1](https://doi.org/10.3847/0067-0049/226/1/1)
- Jorissen, A., Van Eck, S., Van Winckel, H., et al. 2016, *A&A*, 586, A158. doi: [10.1051/0004-6361/201526992](https://doi.org/10.1051/0004-6361/201526992)
- Keenan, P. C. 1993, *PASP*, 105, 905, doi: [10.1086/133252](https://doi.org/10.1086/133252)
- Li, Y. B., Luo, A. L., Du, C. D., et al. 2018, *ApJS*, 234, 31, doi: [10.3847/1538-4365/aaa415](https://doi.org/10.3847/1538-4365/aaa415)
- Liu, C., Cui, W. Y., Zhang, B., et al. 2015, *Research in Astronomy and Astrophysics*, 15, 1137, doi: [10.1088/1674-4527/15/8/004](https://doi.org/10.1088/1674-4527/15/8/004)
- Margon, B., Anderson, S. F., Harris, H. C., et al. 2002, *AJ*, 124, 1651, doi: [10.1086/342284](https://doi.org/10.1086/342284)
- Mauron, N., Azzopardi, M., Gigoyan, K., et al. 2004, *A&A*, 418, 77. doi: [10.1051/0004-6361:20034264](https://doi.org/10.1051/0004-6361:20034264)
- McClure, R. D. 1983, *ApJ*, 268, 264, doi: [10.1086/160951](https://doi.org/10.1086/160951)

- . 1997, *PASP*, 109, 256, doi: [10.1086/133882](https://doi.org/10.1086/133882)
- McClure, R. D., Fletcher, J. M., & Nemec, J. M. 1980, *ApJ*, 238, L35, doi: [10.1086/183252](https://doi.org/10.1086/183252)
- Parada, J., Heyl, J., Richer, H., Ripoche, P., & Rousseau-Nepton, L. 2023, *MNRAS*, 522, 195, doi: [10.1093/mnras/stad965](https://doi.org/10.1093/mnras/stad965)
- Ripoche, P., Heyl, J., Parada, J., & Richer, H. 2020, *MNRAS*, 495, 2858, doi: [10.1093/mnras/staa1346](https://doi.org/10.1093/mnras/staa1346)
- Roulston, B. R., Green, P. J., Montez, R., et al. 2022, *ApJ*, 926, 210. doi:[10.3847/1538-4357/ac4706](https://doi.org/10.3847/1538-4357/ac4706)
- Secchi, A. 1869, *AN*, 73, 129
- Shejeelammal, J., & Goswami, A. 2022, *ApJ*, 934, 110, doi: [10.3847/1538-4357/ac7aac](https://doi.org/10.3847/1538-4357/ac7aac)
- Si, J. M., Luo, A. L., Li, Y. B., et al. 2014, *SCPMA*, 57, 176, doi: [10.1007/s11433-013-5374-0](https://doi.org/10.1007/s11433-013-5374-0)
- Si, J. M., Li, Y. B., Luo, A. L., et al. 2015, *Research in Astronomy and Astrophysics*, 15, 1671, doi: [10.1088/1674-4527/15/10/005](https://doi.org/10.1088/1674-4527/15/10/005)
- Skrutskie, M. F., Cutri, R. M., Stiening, R., et al. 2006, *AJ*, 131, 1163, doi: [10.1086/498708](https://doi.org/10.1086/498708)
- Stephenson, C. B. 1973, *A general catalogue of S stars*
- . 1989, *Publications of the Warner & Swasey Observatory*, 3, 53
- Totten, E. J., & Irwin, M. J. 1998, *MNRAS*, 294, 1, doi: [10.1046/j.1365-8711.1998.01086.x](https://doi.org/10.1046/j.1365-8711.1998.01086.x)
- Totten, E. J., Irwin, M. J., & Whitelock, P. A. 2000, *MNRAS*, 314, 630, doi: [10.1046/j.1365-8711.2000.03370.x](https://doi.org/10.1046/j.1365-8711.2000.03370.x)
- Wang, S., & Chen, X. 2019, *ApJ*, 877, 116, doi: [10.3847/1538-4357/ab1c61](https://doi.org/10.3847/1538-4357/ab1c61)
- Wang, S., & Jiang, B. W. 2014, *ApJ*, 788, L12, doi: [10.1088/2041-8205/788/1/L12](https://doi.org/10.1088/2041-8205/788/1/L12)
- Worthey, G., Faber, S. M., Gonzalez, J. J., & Burstein, D. 1994, *ApJS*, 94, 687, doi: [10.1086/192087](https://doi.org/10.1086/192087)
- Zamora, O., Abia, C., Plez, B., et al. 2009, *A&A*, 508, 909. doi:[10.1051/0004-6361/200912843](https://doi.org/10.1051/0004-6361/200912843)
- Zhao, G., Zhao, Y. H., Chu, Y. Q., Jing, Y. P., & Deng, L. C. 2012, *Research in Astronomy and Astrophysics*, 12, 723, doi: [10.1088/1674-4527/12/7/002](https://doi.org/10.1088/1674-4527/12/7/002)